PROCEEDINGS OF SPIE

SPIEDigitalLibrary.org/conference-proceedings-of-spie

Endoluminal non-contact soft tissue ablation using fiber-based Er:YAG laser delivery

Dennis Kundrat, Alexander Fuchs, Andreas Schoob, Lüder Alexander Kahrs, Tobias Ortmaier

Dennis Kundrat, Alexander Fuchs, Andreas Schoob, Lüder Alexander Kahrs, Tobias Ortmaier, "Endoluminal non-contact soft tissue ablation using fiber-based Er:YAG laser delivery," Proc. SPIE 9702, Optical Fibers and Sensors for Medical Diagnostics and Treatment Applications XVI, 97020E (7 March 2016); doi: 10.1117/12.2211796

SPIE.

Event: SPIE BiOS, 2016, San Francisco, California, United States

Endoluminal Non-Contact Soft Tissue Ablation using Fiber-based Er:YAG Laser Delivery

Dennis Kundrat, Alexander Fuchs, Andreas Schoob, Lüder Alexander Kahrs, Tobias Ortmaier

Gottfried Wilhelm Leibniz Universität Hannover, Faculty of Mechanical Engineering, Institute of Mechatronic Systems, Appelstr. 11a, Hanover, Germany, 30167

ABSTRACT

The introduction of Er:YAG lasers for soft and hard tissue ablation has proven promising results over the last decades due to strong absorption at 2.94 µm wavelength by water molecules. An extension to endoluminal applications demands laser delivery without mirror arms due to dimensional constraints. Therefore, fiber-based solutions are advanced to provide flexible access while keeping space requirements to a minimum. Conventional fiber-based treatments aim at laser-tissue interactions in contact mode. However, this procedure is associated with disadvantages such as advancing decrease in power delivery due to particle coverage of the fiber tip, tissue carbonization, and obstructed observation of the ablation progress. The objective of this work is to overcome aforementioned limitations with a customized fiber-based module for non-contact robot-assisted endoluminal surgery and its associated experimental evaluation. Up to the authors knowledge, this approach has not been presented in the context of laser surgery at 2.94 µm wavelength. The preliminary system design is composed of a 3D Er:YAG laser processing unit enabling automatic laser to fiber coupling, a GeO_2 solid core fiber, and a customized module combining collimation and focusing unit (focal length of 20 mm, outer diameter of 8 mm). The performance is evaluated with studies on tissue substitutes (agar-agar) as well as porcine samples that are analysed by optical coherence tomography measurements. Cuts (depths up to 3 mm) with minimal carbonization have been achieved under adequate moistening and sample movement ($1.5\,\mathrm{mm\,s^{-1}}$). Furthermore, an early cadaver study is presented. Future work aims at module miniaturization and integration into an endoluminal robot for scanning and focus adaptation.

Keywords: laser surgery, soft tissue ablation, endoluminal robot, laser-fiber-coupling, ER:YAG laser

1. INTRODUCTION

The application of erbium-doped yttrium aluminium garnet (Er:YAG) lasers for soft and hard tissue ablation has been subject of various studies in the last decades. Near-infrared Er:YAG sources emit radiation in pulsed or continuous wave mode at a central wavelength of $\lambda = 2.94$ µm based on diode-pumped solid-state electron transitions. This correlates well with the peak absorption wavelength of water molecules contained in biological tissue in high contents leading to small penetration depths and high absorption. Further generic advantages of laser-tissue interactions are dedicated to arbitrary ablation patterns without restrictions due to instrument geometries as well as missing physical contact.

These properties motivated the introduction of laser devices to surgical interventions in order to improve intra-operative performance and post-operative outcome as well as to establish innovative surgical procedures. In the recent years, Er:YAG lasers have been used predominantly with hand-guided systems in bone surgery (e.g. oral or orthopaedic surgery) with promising results regarding minimal thermal damage to surrounding tissue, precise ablation (e.g. cuts or patterns), and superior postoperative healing in comparison to prevalent CO_2 lasers.[1] Nevertheless, studies for treatment of soft tissue have proven applicability and predominantly target dental interventions. A brief summary of related work of *ex vivo* and *in vivo* Er:YAG soft tissue experiments as well as flexible fiber-based laser delivery is provided in the following paragraphs. The overview also highlights important laser parameters such as pulse energy E_p, pulse frequency f_p, pulse duration τ_p, scanning velocity v_S, and extent of thermal damage or heat-affected zone.

Address all correspondence to: Dennis Kundrat, E-mail: dennis.kundrat@imes.uni-hannover.de, Tel: +49 (0)511-762-17845, Fax: +49 (0)511-762-19976

Optical Fibers and Sensors for Medical Diagnostics and Treatment Applications XVI, edited by Israel Gannot
Proc. of SPIE Vol. 9702, 97020E · © 2016 SPIE · CCC code: 1605-7422/16/$18 · doi: 10.1117/12.2211796

Dickinson et al. investigated non-contact interaction of focused pulsed Er:YAG radiation in a variety of cadaveric soft tissues (e.g. brain, liver, and intestine) *ex vivo*.[2] Experiments with single pulse ablation and scanning ($E_P = 100$ mJ, $f_P = 10$ - 30 Hz, $v_S = 0.18$ - 0.35 mm s^{-1}) have been conducted. Histological measurements revealed a thermal and surface damage extending laterally in an average range of 10 - 30 µm with a maximum of 200 µm. More recent experiments ($E_P = 0.1$ - 2 J, $f_P = 5$ Hz) investigated *ex vivo* the influence of crater depth, number of pulses, and ablation dosimetry on porcine skin.[3] The results confirmed the influence of tissue-specific threshold with respect to radiant exposure and ablation depth. Zaffe et al. compared morphological, histochemical, and immunocytochemical changes of human mucosal tissue after *in vivo* CO_2 and Er:YAG laser irradiation.[4] No differences in the healing process of 20 patients after Er:YAG ($E_P = 140$ - 250 mJ, $f_P = 15$ Hz) or CO_2 laser surgery were clinically observed. The damage to epithelial tissue, a low inflammatory reaction, and a quick healing process as well as low scarring occurred in conducted clinical trials. In contrast, CO_2 laser show a better haemostatic capability. A comprehensive study with human *in vivo* trials (n = 31) has shown no complications or side effects as well as no carbonization in manual Er:YAG treatment of oral soft tissue in contact mode ($E_p = 80$ mJ, $f_p = 10$ Hz).[5] These results are associated to the positive influence of a bactericidal effect due to irradiation induced hydroxyl (OH) radicals.[6] Romeo et al. have conducted an evaluation on porcine tongue tissue. A damage zone less than 1 mm was determined histologically even above $E_P = 150$ mJ pulse energy.[7] Very low epithelial, stromal, and vascular damages of bovine oral tissue[8] as well as strongly reduced thermal injury to epithelial and subepithelial tissue in laryngeal surgery[9] are reported recently for irradiation at 2.94 µm. In clinical use, laser radiation has to be delivered from source to target with a maximum of handling comfort to gain the surgeons' acceptance. The most common laser delivering systems are articulated mirror arms in combination with manually guided hand pieces but these restrict potential field of applications (e.g. access of anatomical cavities in endoscopy) due to size constraints and limited flexibility. These restrictions can be circumvented with more flexible fiber-based solutions including solid multimode or hollow core fibers. The latter ones generally show a higher damage threshold and improved flexibility[10] but are also prone to damages without proper tip sealing.[10] In contrast, solid core fibers are fabricated in sapphire, chalcogenides, and GeO_2 and are already analysed as well as partly used in clinical applications due to reliable delivery of high-power laser radiation.[11]

Recent developments in robot-assisted minimally invasive surgery (MIS) motivate our work to consolidate flexible Er:YAG laser delivery and a dexterous robot for non-contact endoluminal soft tissue surgery with integrated stereoscopic imaging.[12] This approach avoids visual occlusions of the ablation progress due to employed fiber in contact mode. Up to the author's knowledge this approach has not been investigated so far and it strongly motivates the development of the focus unit described afterwards. A larger working distance with respect to the robot's tip is required in order to provide overlap with camera's imaging field of view (FOV). Thus, observability with employed camera modules[13] is achieved within at least 18 - 20 mm distance. In the following a description of the preliminary design and experimental evaluation is presented.

2. MATERIALS AND METHODS

2.1 Design and components of focus unit

The design of the focus unit (see Fig. 1) is mainly determined by dimensional constraints with respect to the endoluminal robot as well as available surgical laser and optical fibers for transmission of high-power IR laser radiation. Basically, solid core fibers are considered for reliable laser transmission at 2.94 µm (see Sec. 1). This work uses GeO_2 fibers (Infrared Fibersystems, Silver Springs, MD, USA) with 450 µm core diameter, numerical aperture of 0.12, damping of 0.5 dB m^{-1}, and minimum bending radius of 40 mm. Prior to opto-mechanical assembly, cladding is removed manually and tips are cleaved with a LDC-400 fiber cleaver (Vytran LLC, Morganville, NJ, USA). Afterwards, both tips are cleaned with isopropanol and visually inspected with magnified light microscopy. Additionally, a flexible polytetrafluoroethylen (PTFE) tube covers and protects the raw fiber. A customized stainless steel ferrule is fabricated and glued to one tip in order to establish a mechanical interface to the focus unit. A two-lens layout (see Fig. 1a) is preferred for the proof-of-concept prototype in order to meet dimensional constraints. Consequently, beam shaping optics are required for collimation and focusing of the free beam after fiber transmission to guarantee desired optical properties. Regarding mechanical and optical constraints, subsequent requirements are specified: 1) outer diameter of the module has to be less than 8.5 mm

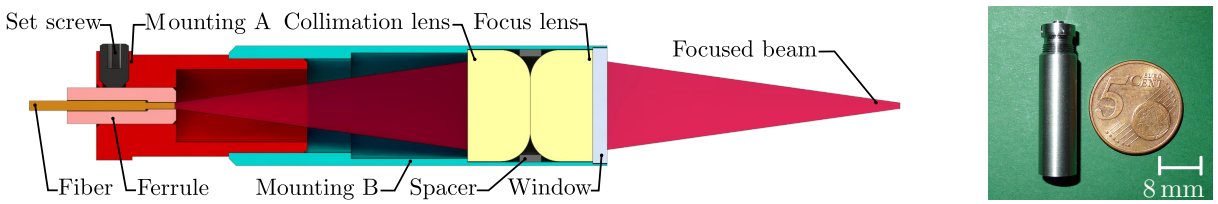

(a) (b)

Figure 1: Design and prototype of proposed focusing unit: (a) Schematic CAD-drawing of the assembly composed of threaded mountings A and B, beam shaping and fiber optics, and protective window. (b) Prototype assembled and manufactured in stainless steel.

2) focal length of approx. 20 mm in order to ensure observability with chip-on-the-tip stereoscopic cameras and 3) Rayleigh-length of approx. ± 2 mm to compensate for adjustment errors due to robot kinematics. The selection of lenses is based on ZEMAX (ZEMAX LLC, Kirkland, WA, USA) simulations in order to obtain the desired focal length at the specified wavelength. Thus, collimation and subsequent focusing is achieved with a pair of two customized plano-convex CaF_2 lenses (LA5315-D, Thorlabs Inc., Newton, NJ, USA) with anti reflective (AR) coating for $\lambda = 1.65 - 3.0\,\mu m$. Both lenses have been processed with optical machining in order to decrease the lens diameter from 12 mm to 7.5 mm. The unit as shown in Fig. 1a and Fig. 1b is composed of two customized manufactured stainless steel tubes represented by mounting A and B, respectively. Both components are threaded to enable precise adjustment of the distance between fiber tip and collimation lens by turning mounting B. Both lenses are inserted and aligned with a circular spacer. An enclosing sapphire window protects mounted components. The ferrule is locked with a set skrew and provides an optical interface for quick replacement of the fiber.

2.2 Experimental set-up

Optical characteristics and ablation performance of the focus unit are evaluated by extending an existing experimental set-up for 3D hard tissue processing[14] to an Er:YAG laser source with automated fiber-coupling. The 3D processing head shown in Fig. 2a is composed of a pulsed Er:YAG solid-state source (DPM 15 laser module, Pantec Engineering/3m.i.k.r.o.n^{TM}, Ruggell, Liechtenstein) emitting the beam to shape-modulating lenses and mirrors in order to finally pass through focus and lateral scanning devices (varioSCAN & hurrySCAN, SCANLAB AG, Purchheim, Germany). A f-θ flat-field lens focuses the beam to $f = 100$ mm resulting in combination with aforementioned scanning devices in a focal workspace of 10 x 10 x 10 mm. A quick exchange fiber chuck (FPH-DJ, Newport Corporation, Irvine, CA, USA) is used to coarsely position the tip of the fiber in the center of the described focal workspace.

2.3 Laser-to-fiber coupling

The aim of the aforementioned set-up is to automatically align laser beam and fiber tip for efficient coupling as well as minimal installation time by using lateral and axial focal point (approx. 360 µm diameter) displacement of the 3D laser scanning unit. Several contributions have already addressed the opto-mechanical alignment problem between two optical components by proposing methods and algorithms based on powermeter sensor readings and multi-axes optical stages for independent translation and rotation of two facing fiber ends.[15] Generally, one optical component is fixed and the second optical component is manipulated in multiple degrees of freedom. Apart from recent approaches transferring the alignment problem to an optimization problem and model solved by Hamiltonian, Simplex, and particle swarm algorithms,[15] this work adopts an ascend/descent-based (Hill-Climb) method based on persistent sensor readings of the power meter in combination with displacements of the 3D scanning unit to reduce complexity. The tip of the fiber is coarsely positioned in the aforementioned workspace. Additionally to continuously measured and processed pyroelectric powermeter data (4π power meter, Laserpoint srl, Vimodrone, Italy) at the tip of the fiber, the proposed Hill-Climb method includes the following steps: 1) Coarse lateral scanning (step-width 100 µm until rising power signal is detected. 2) Lateral fine scan starting from position in 1) towards increasing signal (step-width 50 µm). 3) Stop procedure if power signal

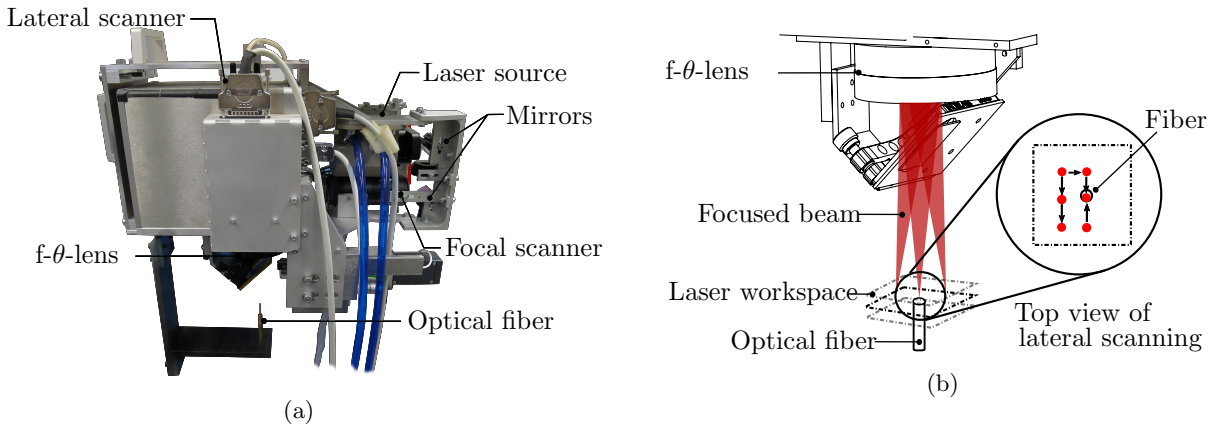

Figure 2: Opto-mechanical set-up for automatic laser-fiber coupling: a) Photography of 3D laser scanning device with laser source, beam shaping optics, scanning units, and fiber mounting. b) Magnified schematics of laser workspace and associated lateral scanning pattern for laser-fiber-coupling.

convergence to maximum power delivery is achieved. The method was evaluated with repeated re-assembly and coarse positioning of the fiber in the workspace (n=10). Afterwards the aforementioned algorithm was utilized to obtain laser-fiber coupling. The approach failed in one trial due to placement at workspace boundary. The average runtime in residual trials until signal convergence was approx. 173±16 s. In reference to an initial source power of 1 W, an average coupling efficiency of 54±8 % was achieved correlating to results of Poletto et al.[11]

2.4 Optical characterization of the focus unit

Optical properties of the focus unit (e.g. beam caustics) are determined by applying the established knife-edge technique[16] partly in accordance to ISO-11146 standard. Prior to evaluation, the unit was assembled and distance between mounting A and B was set according to simulation results. Under the assumption of a Gaussian beam profile, the measurement is conducted with translation of a sharp-edged blade (e. g. razor blade) perpendicular to the beam propagation direction at specific distances. Thus, the blade covers the incident beam incrementally by partly blocking radiation. Simultaneously, residual laser power is measured for each translational step (width 50 µm) with aforementioned powermeter. Afterwards, obtained data is fitted to an error function and $1/e^2$-radius is estimated. This procedure is repeated five times within a range of ± 4 mm with respect to the focal length of 20 mm in steps of 0.5 mm in order to obtain the beam caustics around the focal point. The overall set-up is shown in Fig. 3a. Lateral and axial translation of the blade with respect to the focus unit are performed with a hexapod robot (H-824, Physik Instrumente (PI), Karlsruhe, Germany). Based on acquired data and aforementioned standards one can estimate the beam waist location to $z_0 = 18.65$ mm in reference to the tip of the module. Considering a protective windows thickness of 1 mm the resulting location of $z_{0*} = 19.65$ mm is closed to specified position of 20.00 mm. Furthermore, the Rayleigh-length is estimated to $z_R = \pm 1.75$ mm and the beam waist diameter to $2w_0 = 506$ µm. The half-angle beam divergence is calculated to $\theta = 0.124$ rad.

2.5 Ablation experiments

The performance of the developed focus unit is evaluated with experiments on tissue substitutes (agar-agar) and porcine specimens. Prior to experiments agar-agar samples (4%) were produced in accordance to manufacturer instructions (BIOVITA GmbH, Hamm, Germany). Afterwards, produced specimens are transferred to petri dishes and stored in a refrigerator in order to maintain a balanced water content and avoid dehydration induced shrinkage. Fresh porcine samples are obtained and immediately resectioned in smaller samples. Subsequently, all porcine samples are stored in petri dishes and continuously moistened with saline solution in a refrigerator. This work employs the aforementioned hexapod (see Fig. 3a) to simulate a scanning movement of the laser. The focus unit is attached to the hexapod platform and the specimen surface is positioned statically in the focal range of the unit. Afterwards, the platform conducts a translational single axis movement ($v_S = 1.5\,\mathrm{mm\,s^{-1}}$). For preliminary evaluation of ablation performance, the laser settings are set to constant pulse duration $\tau_P = 200$ µs

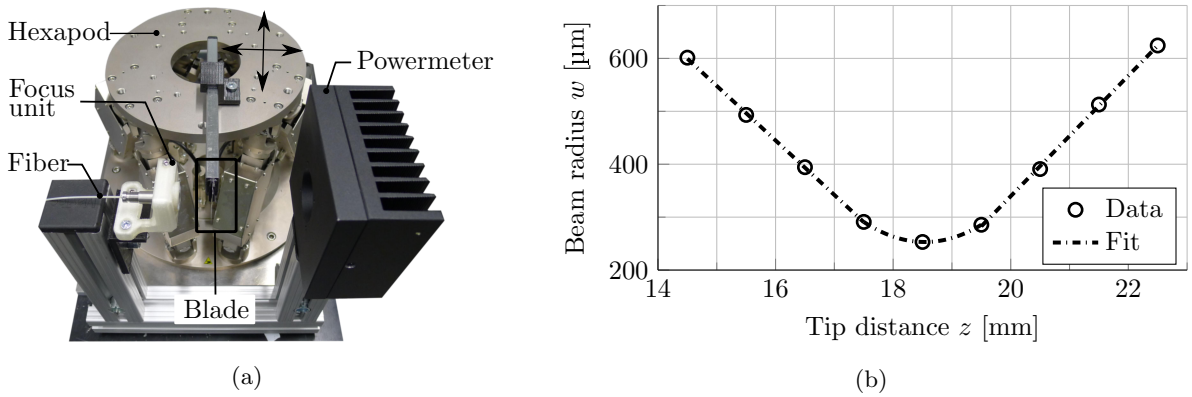

(a) (b)

Figure 3: Experimental set-up for knife-edge measurements and associated beam caustics of focus unit. a) Component layout to characterize experimentally the optical performance of the developed focus unit. A hexapod device is employed for high-resolution translation of the edge. b) Beam caustics of designed unit around experimentally determined focal point. Data is fitted in accordance to ISO-11146. Standard deviation (not shown) of each data point is below 25 µm.

and diode current $I_P = 200$ A. Pulse frequencies are varied from $f_P = 30$ - 80 Hz for both types of tissue. Multiple passes (n = 2 - 4) are applied with continuous moistening. Five linear ablations (cuts) are conducted for each set of parameters and tissue with a length of approx. 15 mm. Afterwards, each specimen in analysed by swept-source optical coherence tomography (OCT) (OCs1300, Thorlabs Inc., NJ, USA). A volume dataset of each ablation is acquired and the incision profile is measured manually in width and depth at 20 specific positions along the propagation axis.

2.6 Pre-clinical cadaver study

An early design of the proposed focus unit was evaluated qualitatively in a pre-clinical cadaver study in the Anatomy Laboratory of University Hospital Besaçon, France. Two fresh frozen cadavers (male and female) have been selected in accordance with ethics approval. Components and optical set-up were similar to the aforementioned laboratory scenario (see Sec. 2.2) except of an replacement of the 3D scanning unit with manual stages for adjustments of employed fiber coupling lenses due to simplified installation. The unit was applied manually to oral soft tissue of selected cadavers and ablation was monitored with the integrated chip-on-the-tip stereoscopic camera.

3. RESULTS

In reference to determined optical properties of the focus unit and laser parameters, the presented set-up (including coupling losses) enables a pulse energy of approx. $E_P = 10$ mJ and a focal diameter of $2w_0 = 506$ µm resulting in an average radiant exposure of $J_P = 50\,\mathrm{mJ\,mm^{-2}}$ for a single pulse within the focal range. The pulse overlap n_P during scanning movement is greater than 85% for all experiments.

The results of the experimental evaluation of the focus unit on tissue substitutes (agar-agar) and porcine tissue are summarized in Fig. 4. As shown in Fig. 4a and Fig. 4c , the relationship of increasing pulse frequencies f_P and adjunct rising pulse overlap n_P on the ablation depth can be assumed to be linear. The results further reveal that the application of increasing pulse frequencies on porcine tissue is associated to larger ablations depths compared to employed tissue substitute. In both scenarios additional passes result in increasing ablation depths. Maximum depths of approx. 1.75 mm on agar-agar and approx. 2.8 mm on porcine tissue were achieved with four passes at $f_P = 80$ Hz. Additionally, one can observe a larger standard deviation in porcine samples. The linear relationship between pulse frequency and increasing ablations depth is in correlation with results of Zhang.[3] The difference in standard deviations is expected to be based on less homogeneous tissue properties (e.g. water content) of porcine tissue in contrast to agar-agar. This results in larger deviations while performing OCT-based ablation measurements. In contrast, Fig. 4b and Fig. 4d describe the influence of pulse frequency f_P and number of passes on the ablation width w.r.t. agar-agar as well as porcine samples. In comparison to porcine samples,

the relationship between ablation width and frequency can be assumed to be non-linear for agar-agar samples. The effect is less dominant in porcine samples. One can expect a stronger shrinkage in porcine tissue resulting in less increasing width compared to agar-agar. However, the maximum width in both scenarios is below 0.9 mm. The standard deviation is in equivalence to measurements of the ablation depth of porcine specimens increased. No carbonization or charring (significant change of tissue color) has been detected after laser ablation with light microscopy (magnification of 10x) analysis or OCT. In porcine samples surrounding tissue has partially shown shrinkage due to thermal interaction and water evaporation.

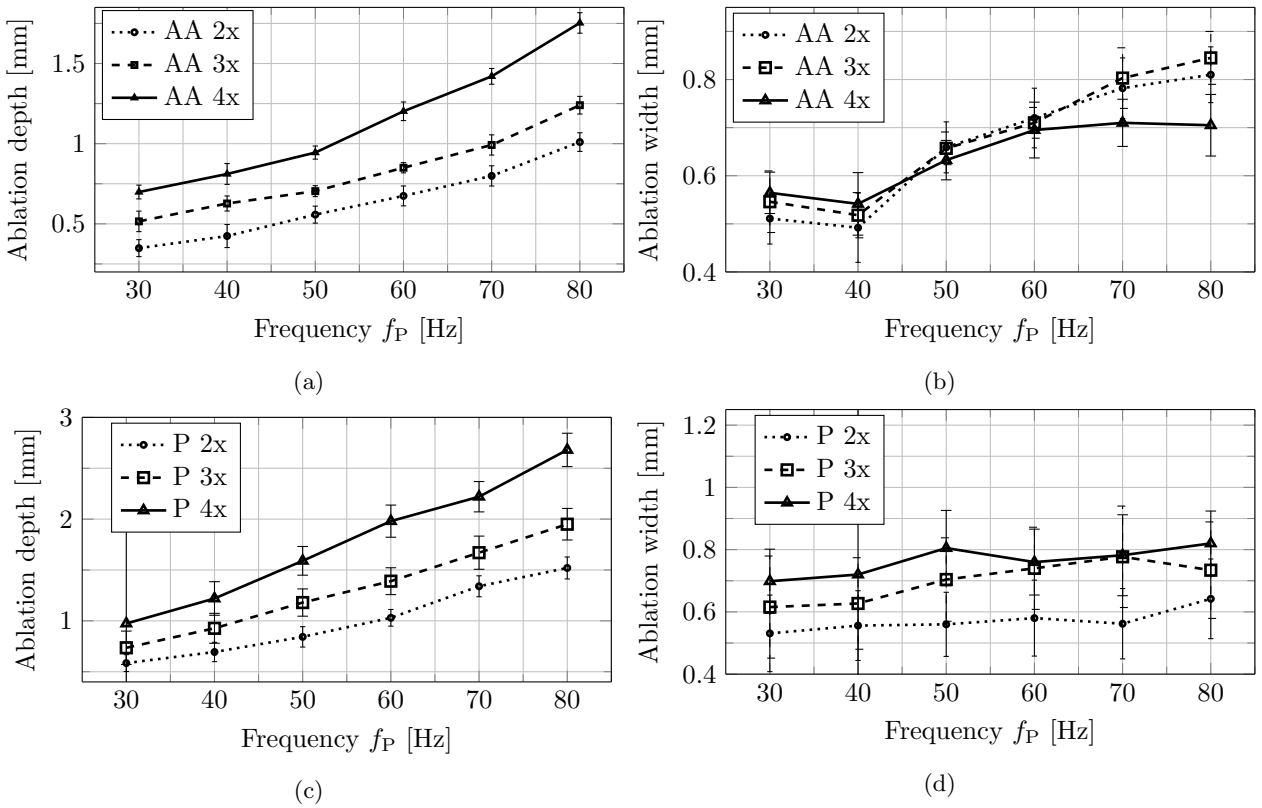

Figure 4: Experimental results of ablation width and depth measurements on agar-agar (AA) and porcine (P) samples in relationship to pulse frequency and number of passes: a) Ablation depth on agar-agar specimens with approximately linear relation of frequency, passes, and depth. b) Ablation width on agar-agar samples demonstrating non-linear relationship between width, frequency, and number of passes. c) Ablation depth on porcine samples shows similar relationship of pulse frequency and ablation depth as presented in a) with increasing slope. d) Influence of increasing pulse frequency on ablation width on porcine samples shows less effect in comparison to results of b).

Preliminary results of the cadaver trial are presented in Fig. 5a. Both images show the progress of manually guided and adjusted ablations employing the aforementioned optical set-up. Both experiments were conducted with an average power of approx. 1.5W. After oral insertion, a scanning movement was simulated by moving the tip translationally. One can observe a continuous ablation after laser activation. Furthermore, the images reveal the influence of scanning velocity and pulse frequency due to a carbonization tendency if the velocity is chosen to low. Thus, the pulses overlap resulting in local thermal accumulation and subsequent carbonization. Fig. 5b is related to a 3D reconstruction based on the employed stereoscopic image acquisition. This feature allows for real-time monitoring of the ablation progress and estimation of incision length. Furthermore, dense 3D surface information enables to adjust the focal spot on the tissue.

(a) (b)

Figure 5: Qualitative results of first cadaver trial: a) Images acquired in two cadavers with internal chip-on-the-tip camera system showing progress of manually guided ablations of oral soft tissue. b) 3D reconstructed surface (colored pointclound) based on stereoscopic image data showing incision and Euclidean distance measurement indicated by small spheres.

4. CONCLUSION

This work presents first steps towards design, manufacturing, and experimental evaluation of a focus unit for robotic non-contact endoluminal surgery. Design and employed components are described and subsequent optical characterization has validated simulation results. The use of an existing hard tissue laser processing unit addresses the aspect of versatility and enables to perform an automatic laser-to-fiber coupling process. The experimental evaluation on porcine tissue as well as substitutes (agar-agar) confirmed applicability of Er:YAG laser radiation for non-contact soft tissue surgery in accordance with reviewed literature. Future work is dedicated to integration and further miniaturization of the module. Additionally, extensive experiments regarding soft tissue ablation performance are foreseen. In this regard, single and multi pulse interactions are analysed in order to determine optimal laser settings for minimizing tissue trauma.

ACKNOWLEDGMENTS

This work has been funded by European Union Seventh Framework Programme FP7/2007-2013 under grant agreement µRALP - n^o 288663. We further thank our students Vikram Katti and Alexander Michailik for their experimental work and assistance in data processing. Moreover, we grateful appreciate the support of Karl Storz GmbH & Co. KG for providing optical components including a laser source, Infrared Fibersystems for fiber samples, and the Laser Zentrum Hannover e.V. for help with fiber cleaving.

REFERENCES

[1] de Mello, E., Pagnoncelli, R., Munin, E., Filho, M., de Mello, G., Arisawa, E., and de Oliveira, M., "Comparative histological analysis of bone healing of standardized bone defects performed with the er:yag laser and steel burs," *Lasers in Medical Science* **23**(3), 253–260 (2008).

[2] Dickinson, M., Charlton, A., King, T., Freemont, A., and Bramley, R., "Studies of Er-YAG laser interactions with soft tissue," *Lasers in Medical Science* **6**(2), 125–131 (1991).

[3] Zhang, X., Xie, S., Ye, Q., and Zhan, Z., "An Observation of Ablation Effect of Soft Biotissue by pulsed Er:YAG Laser," *Proc. of SPIE*, **6435** (2007).

[4] Zaffe, D., Vitale, M. C., Martignone, A., Scarpelli, F., and Botticelli, A. R., "Morphological, Histochemical, and Immunocytochemical Study of CO2 and Er:YAG Laser Effect on Oral Soft Tissues," *Photomedicine and Laser Surgery* **22(3)**, 185–189 (2004).

[5] Watanabe, H., Ishikawa, I., Motoyuki, S., and Hasegawa, K., "Clinical Assessments of the Erbium:YAG Laser for Soft Tissue Surgery and Scaling," *Journal of Clinical Laser Medicine and Surgery* **14**, 67–75 (1996).

[6] Lubart, R., Kesler, G., Lavie, R., and Friedmann, H., "Er:YAG Laser promotes Gingival Wound Repair by Photo-Dissociating Water Molecules," *Photomedicine and Laser Surgery* **23**, 369–372 (2005).

[7] Romeo, U., Libotte, F., Palaia, G., Del Vecchio, A., Tenore, G., Visca, P., Nammour, S., and Polimeni, A., "Histological in vitro evaluation of the effects of er:yag laser on oral soft tissues.," *Laser Med Sci* **27**, 749–753 (2012).

[8] Merigo, E., Clini, F., Fornaini, C., Oppici, A., Paties, C., Zangranadi, A., Fontana, M., Rocca, J.-P., Meleti, M., Manfredi, M., Cella, L., and Vescovi, P., "Laser-assisted surgery with different wavelengths: a preliminary ex vivo study on thermal increase and histological evaluation," *Laser Med Sci* **28**, 497–504 (2013).

[9] Böttcher, A., Jowett, N., Kucher, S., Reimer, R., Schumacher, U., Knecht, R., Wöllmer, W., Mänscher, A., and Dalchow, C., "Use of a microsecond Er:YAG laser in laryngeal surgery reduces collateral thermal injury in comparison to superpulsed CO2 laser," *European Archives of Oto-Rhino-Laryngology* **271**, 1121–1128 (2014).

[10] Urich, A., Maier, R., Fei, Y., Knight, J., Hand, D., and Shephard, J., "Flexible delivery of Er:YAG radiation at 2.94 μm with negative curvature silica glass fibers: A new solution for minimally invasive surgical procedures.," *Biomedical Optics Express* **4**(2) (2013).

[11] Poletto, T., Ngo, A. K., Tchapyjnikov, A., Levon, K., Tran, D., and Fried, N. M., "Comparison of germanium oxide fibers with silica and sapphire fiber tips for transmission of erbium: Yag laser radiation," *Lasers in Surgery and Medicine* **38**, 787–791 (2006).

[12] Kundrat, D., Schoob, A., Kahrs, L., and Ortmaier, T., [*Soft Robotics*], ch. Flexible Robot for Laser Phonomicrosurgery, 265–271, Springer-Verlag Berlin Heidelberg (2015).

[13] Schoob, A., Kundrat, D., Kahrs, L. A., and Ortmaier, T., "Comparative study on surface reconstruction accuracy of stereo imaging devices for microsurgery," *International Journal of Computer Assisted Radiology and Surgery (JCARS)* (2015).

[14] Fuchs, A., Pengel, S., Bergmeier, J., Kahrs, L., and Ortmaier, T., "Fast and automatic depth control of iterative bone ablation based on optical coherence tomography data," *Proc. SPIE 9542, Medical Laser Applications and Laser-Tissue Interactions VII*, (2015).

[15] Yu, M.-T., Lin, T.-Y., Li, Y.-Y., and Shu, P.-F., "Study on the optimization methods for optomechanical alignment," *Proc. of SPIE Vol. 6289*, (2006).

[16] De Arajo, M. A., Silva, R., De Lima, E., Pereira, D. P., and De Oliveira, P. C., "Measurement of gaussian laser beam radius using the knife-edge technique: improvement on data analysis," *Applied Optics* **48**, 393–396 (2009).